SECONDARY CRATERS AND EJECTA ON ICY SATELLITES: SIZE-VELOCITY DISTRIBUTIONS. Kelsi N. Singer[1], Luke Nowicki[1], William B. McKinnon[1], and Paul M. Schenk[2]. [1]Department of Earth and Planetary Sciences and McDonnell Center for the Space Sciences, Washington University in St. Louis, MO 63130 (ksinger@levee.wustl.edu, mckinnon@wustl.edu); [2]Lunar and Planetary Institute, Houston, TX 77058.

Introduction: Europa provides a unique case study for investigating secondary cratering processes. Europa's young, relatively un-cratered surface is ideal for mapping secondaries from a given large primary [1-4]. This work looks specifically at size-velocity distributions on Europa and elsewhere, to determine the largest size fragments that might be ejected from an icy satellite by a given impact. The case study described here is for the Tyre impact basin on Europa. At ~44 km in diameter, with graben extending out to ~175 km in diameter, Tyre is the largest basin on Europa. We estimate the size and velocity of ejected fragments that formed Tyre's secondaries. A power-law curve fit to the largest fragments for a given velocity is compared to that found for Pwyll [5]. We also measured the size-frequency of secondary craters as a function of radial distance from the center of Tyre. Relations of this general form serve as a test of spallation models [6], and guide estimates of the sesquinary-forming impactor population [2,7].

Methods: The image coverage in the Tyre region provides both a broad region around Tyre at medium resolution and a high resolution inset for counting smaller craters and examining secondary morphology. The medium resolution basemap is composed of the nine Galileo frames of the Tyre region with a resolution of ~170 m/px and high incidence and phase angles (~70° and ~80°, respectively). For this map, a lower limit of five pixels was used for identification of craters, which equates to ~850 m. Secondary crater diameters were measured geodesically in ArcGIS. There are several instances of clustered secondaries and secondaries arranged linearly. Where it was possible to distinguish individual craters they were mapped as such. Approximately 1,000 craters above the five-pixel limit were mapped.

A higher resolution, ~30-m/px inset was also mapped. In this mosaic, the background "noise" from lineaments, chaos and general surface roughness became a factor along with resolution in identifying the smallest craters. Also, the incidence and phase angles were low (~30° and ~3°, respectively), which is not ideal for mapping based on topography. The smallest craters identified here were ~200 m, or ~7 times the pixel size. Approximately 375 craters were identified in this scene.

This work follows a similar method to those of Vickery for large craters on Mercury, the Moon and Mars [8,9] and Alpert and Melosh for Pwyll on Europa [5]. As the original location of ejected fragments is imprecisely known, the center of Tyre was used for all distance calculations as a first appoximation [cf. 10]. This leads to an overestimate of the range and thus a modest overestimate of the ejection velocities.

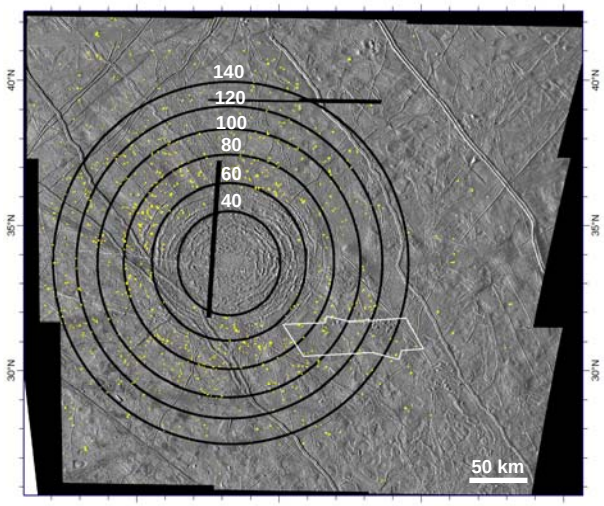

Figure 1. Map of Crater Locations. The resolution of the basemap is 170 m/px. Black rings mark 20 km range intervals, starting at 40 km in radius and extending to 140 km in radius. The white outline marks the location of higher resolution inset (~27 m/px).

The distances are calculated using a flat plane approximation due the short distances involved. For a ballistic trajectory, the relationship is

$$R = (\upsilon_{ej}^2 / g)\sin(2\theta) \quad , \quad (1)$$

where R is the distance from the primary, θ is the ejection angle (assumed to be 45° and also equal to the impact angle), g is surface gravity (1.31 m/s^2), and υ_{ej} is the ejection velocity.

The size of ejected fragments was estimated from Schmidt-Holsapple crater scaling relationships [e.g., 11]. Two scenarios, both for the gravity-dominated regime [11], were considered [as in 8]. One, where the surface is hard and non-porous, is described by

$$d = 0.76 D_{obs}^{1.2} (\sin\theta)^{-0.41} (g/U^2)^{0.205} \quad , \quad (2)$$

where d is the fragment diameter (assuming a spherical ejecta fragment), D_{obs} is the measured secondary crater diameter, and U is impact velocity (the same as ejection velocity, υ_{ej}). Although we consider the non-porous case to be the more appropriate for Europa given the surface is relatively geologically youthful,

we also consider a second scenario, where the surface is granular and porous (sand-like), described by

$$d = 0.753 D_{obs}^{1.28} (\sin\theta)^{-1/3} (g/U^2)^{0.277}. \quad (3)$$

Results: The size-frequency distribution of craters based on their radial distance from Tyre's center is shown in Fig. 2. Cumulative power-law slopes for the craters located in 20 km radial range bins (see Fig. 1) range from approximately –4 to –6, with the total population having a slope of –5 (clearly consistent with secondary distributions generally [12]).

Ejection velocity is plotted against fragment diameter in Fig. 3. The most distant secondaries, at ~290 km, are limited by image coverage. This gives a highest observed ejection velocity (υ_{ej}) of ~650 m/s. The largest fragments (d_{max}) are comparable with those from the 55-km-diameter lunar crater Aristillus [8], but larger than those from 39-km-diameter Harpalus [9], and all correspond to gravity-regime impacts [11]. Curves of the form $d_{max} = a\ \upsilon_{ej}^{-b}$ were fit to the group of maximum fragment sizes across the velocity range, where both d_{max} and υ_{ej} are in MKS units. For the non-porous case $d_{max} = 6.9\text{x}10^5\ \upsilon_{ej}^{-1.17}$ and for the porous case $d_{max} = 3.0\text{x}10^5\ \upsilon_{ej}^{-0.99}$. The fit for d_{max} as a function of υ_{ej} is similar to that found for Pwyll [5]. The coefficient a is the same order of magnitude but ~2 times the value for Pwyll, which might be expected for a primary crater ~2 times larger. The a values for the 2 europan craters are up to several orders of magnitude smaller than a values for craters on Mercury, the Moon or Mars (these range from 10^6-to-10^9) [8,9], but the velocity dependence must be factored in as well.

Discussion: We cannot confirm the preliminary finding of [5] that secondary-crater-forming ejecta on Europa are generally smaller, all other things being equal, than secondary-forming fragments on rocky bodies. This may be due to geological variability (target properties matter), but should be further tested on other icy satellites (e.g., Ganymede). We do find a similar maximum fragment-size-velocity dependence as [5], one remarkably similar to that derived from spallation theory (b = 1.2 [12]), especially for the non-porous (hard ice) case.

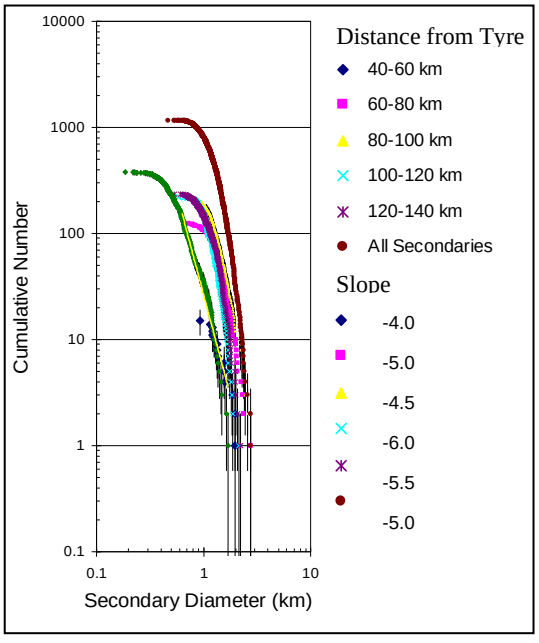

Figure 2. Size-frequency distributions for secondary craters in 20 km radial range bins.

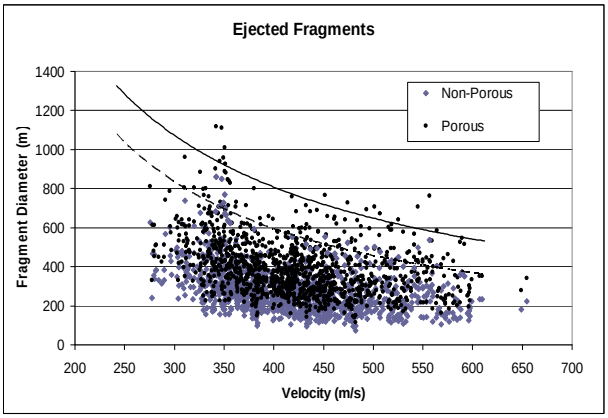

Figure 3. The velocities calculated from the distance from the center of Tyre are compared with fragment diameters calculated from the size of the secondaries. Curves of the form $d_{max} = a\ \upsilon_{ej}^{-b}$ were fit to the maximum fragments sizes: the dashed line represents estimates for a non-porous surface and the solid for a porous one.

As noted above, the Tyre secondaries in Fig. 1 all formed in the gravity regime, so strength effects should not be important. For the slower, larger secondary fragments, however, the gravity-scaled sizes are large enough that the point-source approximation may not hold. Moreover, the Hugoniot elastic limit for ice may only just be exceeded. Such effects may help explain the overall shallowness of the secondaries at Tyre [4].

A simple extrapolation of the d_{max} equations for Tyre and Pwyll to the escape velocity (~2 km/s) gives fragment sizes of 93 m and 34 m, respectively. This is an upper limit on fragment size, as even smaller fragments would be ejected at higher velocities. These would thus produce small craters were they to subsequently impact Europa or another Jovian moon.

References: [1] Bierhaus E.B. et al.. (2005) *Nature 437*, 112 5-1127. [2] Zahnle K.J. et al. (2008) Icarus, 194, 660-674. [3] Bierhaus E.B. et al. (2009) in *Europa* (Pappalardo R.T. et al., eds.) Univ. Ariz. Press. [4] Bierhaus E.B. and Schenk P.M. (2010) *JGR 115*, E12004. [5] Alpert A.J. and Melosh H.J. (1999) *LPSC XXX*, abs. #1881. [6] Melosh H.J. (1984) *Icarus 59*, 234-260. [7] Alvarellos J.L. et al. (2002) *Icarus 160*, 108-123. [8] Vickery A.M. (1986) *Icarus 67*, 224-236. [9] Vickery A.M. (1987) *GRL 14*, 726-729. [10] Housen K.R. and Holsapple K.A. (2011) *Icarus*, in press. [11] Holsapple K.A. (1993) *AREPS 21*, 333-373. [12] McEwen AS. and Bierhaus E.B. (2006) *AREPS 34*, 535-567.